Geoderma 162 (2011) 151–158

Contents lists available at ScienceDirect

Geoderma

journal homepage: www.elsevier.com/locate/geoderma

Mapping depth-to-clay using fitted multiple depth response curves of a proximal EMI sensor

Timothy Saey *, Marc Van Meirvenne, Philippe De Smedt, Liesbet Cockx, Eef Meerschman, Mohammad Monirul Islam, Fun Meeuws

Research Group Soil Spatial Inventory Techniques, Department of Soil Management, Ghent University, Coupure 653, 9000 Gent, Belgium

ARTICLE INFO

Article history:
Received 12 February 2010
Received in revised form 18 January 2011
Accepted 21 January 2011
Available online 19 February 2011

Keywords:
DUALEM-21S
Electromagnetic induction
Paleolandscape
Depth modelling
Depth response functions
Soil map
Depth inversion

ABSTRACT

As an alternative for the depth response approximations based on the theoretical Maxwell's equations, a procedure was proposed to fit depth response curves for different coil configurations. A 39 ha study area was selected in the Belgian loess belt, where loess material was situated on a Tertiary substrate. A survey with the DUALEM-21S electromagnetic induction instrument was carried out to map the depth-to-clay (z_{clay}). The depth response curves were fitted both for the vertical and perpendicular coil configurations using 85 depth observations of z_{clay}.
The resulting depth response curves $R(z_{clay})$ were:

$$R_{p,s}(z_{clay}) = 0.8135 \cdot e^{-1.4131 \cdot \left(\frac{z_{clay}}{s}\right)}$$

for the perpendicular coil configuration (with s as the intercoil spacing) and

$$R_{v,s}(z_{clay}) = 0.9802 \cdot e^{-0.8102 \cdot \left(\frac{z_{clay}}{s}\right)}$$

for the vertical coil configuration.
A set of 4 equations based on the developed depth response functions was used to model z_{clay} at each of the 209 400 measurement points. These z_{clay} predictions were validated using geo-electrical imaging. With two multi-electrode resistivity arrays, z_{clay} was 1D-inverted at 95 locations along two transects, assuming a two-layered soil system. A coefficient of determination of 0.95, with a root mean-squared estimation error of 0.22 m, was found between the predicted and 1D-inverted depths. This procedure allowed the accurate 3D-reconstruction of the paleolandscape before the deposition of the loess. Flow lines were modelled on this paleosurface, revealing past or subsurface stream patterns not visible on the present relief.

1. Introduction

Electromagnetic induction (EMI) instruments measure a depth-weighted average of the soil electrical conductivity. Quantitative applications of EMI sensors to subsoil investigations depend on the ability to transform the measured apparent electrical conductivities (ECa) into horizontal and vertical variations of relevant soil properties such as soil type, soil horizons, soil water storage and soil organic matter (Domsch and Giebel, 2004; Saey et al., 2009b; Tromp-van Meerveld and McDonnell, 2009). Although useful for looking at lateral spatial variation, the ECa gives limited information on how conductivity varies with depth (Pellerin and Wannamaker, 2005). Generally, the propagation of EMI radiation into the soil is described by Maxwell's equations (Reynolds, 1997). The relative response to the primary magnetic field created by the EMI instruments varies with depth and is therefore expressed as a depth response function. This response function is the weighting function for the ECa (= depth-weighted conductivity) (Morris, 2009).

McNeill (1980) defined the depth response functions of EMI instruments in homogeneous soils by asymptotic approximations of the Maxwell's equations. Hendrickx et al. (2002) proved these approximations to be valid in heterogeneous soils. They are based on the assumption that the induction number (β) is very small (Spies and Frischknecht, 1991). This is equivalent to stating that the current that flows in any loop of the magnetic field is completely independent of the current that flows in any other loop since they are not magnetically coupled (McNeill, 1980). The induction number is the ratio of the intercoil separation s to the skin depth δ. This skin depth is defined as the

* Corresponding author. Tel.: +32 92646042; fax: +32 92646247.
E-mail address: imothy.Saey@UGent.be (T. Saey).

0016-7061/$ – see front matter © 2011 Elsevier B.V. All rights reserved.
doi:10.1016/j.geoderma.2011.01.015

distance at which the propagating magnetic field strength has been attenuated to e^{-1} of the strength at the surface and varies inversely with the ECa at low frequencies. Within the restriction of a small β, the McNeill approximation (1980) holds which means that the instrument output is proportional to the ECa and the depth response functions are independent of ECa (Hendrickx et al., 2002). However, Callegary et al. (2007) proved with numerical models based on Maxwell's equations that the depth response can be altered by soil properties affecting the ECa. Especially under high electrically conductive conditions, the simulated depth response function deviates from the function predicted from the McNeill (1980) approximation.

Saey et al. (2009a) used the depth response curves of McNeill (1980) and Dualem Inc. (2007) based on Wait (1962) for the vertical and perpendicular coil configurations to predict the depth-to-clay (z_{clay}) in a two-layered soil. Monteiro Santos et al. (2010) used a one-dimensional, laterally constrained algorithm to invert field-measured ECa data collected with a DUALEM-421S instrument. A forward modelling subroutine, based on the cumulative response from McNeill (1980) was used to calculate the apparent conductivity response of the model. Low z_{clay} values were associated with high ECa values and corresponding high β what makes the asymptotic approximations for the theoretical depth response functions deviating from the real depth response. On the other hand, different numerical inversion simulations based on Maxwell's equations fail to handle the depth functions for the perpendicular coil configurations. Therefore, the objective of this study was to fit depth response curves for different EMI coil configurations in a two-layered soil and apply these to map z_{clay} in a study area within the Belgian loess belt.

2. Materials and methods

2.1. Study area

In Belgium, the Weichselian Pleistocene loess belt occupies a low plateau (altitude 50–200 m) across the central part of the country (Fig. 1). In the loess belt, plateaus alternate with rolling hills and valleys. The mean annual temperature is about 10 °C, while annual precipitation ranges from 700 to 900 mm (Hufty, 2001).

The 39 ha research area was located in Heestert (Belgium) (Fig. 1). It is situated on a southeast facing hillside with an elevation ranging between 25 to 45 m above sea level (a.s.l.). The site consists of eleven neighbouring arable fields (central coordinates: 50º47′58″N, 3º24′41″E). On the national soil map (scale 1:20,000), the soil series of the study area are characterized by a shallow or deeper clay substrate, a silt loam topsoil texture, moderately wet conditions and a textural B-horizon. This soil type corresponds to a loess-derived Haplic Luvisol (World Reference Base, 1998), which is characterized by an argic horizon ranging from 0.3–0.35 m up to 1.3–1.4 m in depth. Initially, the deposited loess was calcareous, but it decalcified mostly to a depth of 2–2.5 m (Hubert, 1976). Generally, a two-layered soil system is acceptable with silty-loess material above a clayey substrate.

2.2. DUALEM-21S electromagnetic induction sensor

In its simplest configuration, a proximal EMI soil sensor consists of two coils separated by a given fixed distance which is put on top of a soil. A primary magnetic field (H_p) is created by the transmitting coil. This field creates eddy currents in the soil below, which induce their own magnetic field (H_i). The induced secondary field is superimposed on the primary field and both H_p and H_i are measured by the receiving coil (McNeill, 1980; Saey et al., 2009b). From this response the ECa of the bulk soil can be obtained. We used the DUALEM-21S instrument (DUALEM Inc., Milton, Canada) which consists of one transmitter coil and four receiver coils located at spacings of 1, 1.1, 2 and 2.1 m. The 1 and 2 m transmitter-receiver pairs form a vertical dipole mode (1 V and 2 V); while the 1.1 and 2.1 m pairs form a perpendicular dipole mode (1.1P and 2.1P) (see Saey et al., 2009a for schematic overview). McNeill (1980) provided a simple form of vertical sensitivity analysis using his cumulative depth response. Cumulative depth response (R) can be used to determine the sensitivity of EMI instruments to all material above or below a given depth. Depths are normalized to facilitate comparisons of

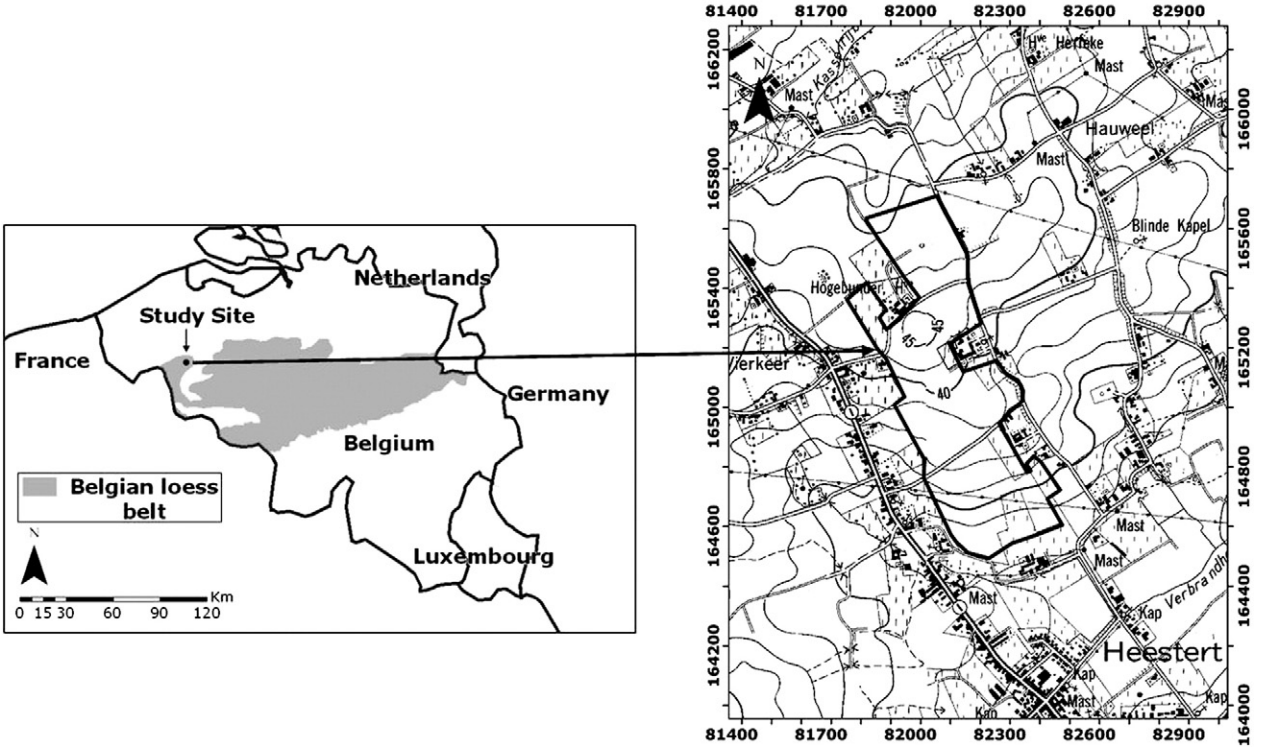

Fig. 1. Localisation of the study area in the Belgian loess belt and topographic map with indication of the boundaries (coordinates are according to the Belgian metric Lambert 72 projection).

different intercoil separations. The normalized depth is the actual depth (z) divided by the intercoil separation (s) (Callegary et al., 2007). An R value represents the fraction of the secondary field at the receiver that originates between the normalized depth $\left(\frac{z}{s}\right)$ and infinite depth. Saey et al. (2009a) found the resulting depths of exploration (DOE) increasing for the different coil configurations of the DUALEM-21S: 1.1P (0.54 m), 2.1P (1.03 m), 1 V (1.55 m) and 2 V (3.18 m). The ECa measurements of the different coil configurations are denoted as: $ECa_{p,1.1}$ for the 1.1P coil configuration, $ECa_{p,2.1}$ for the 2.1P coil configuration, $ECa_{v,1}$ for the 1 V coil configuration and $ECa_{v,2}$ for the 2 V coil configuration.

2.3. ECa survey

The soil ECa of the study area was recorded with the DUALEM-21S soil sensor. The sensor was put in a non-metal sled and pulled behind an all-terrain vehicle at about 10 km h^{-1} crossing the field at parallel lines 4 m apart. In order to obtain estimates of the ECa at unsampled locations, ordinary point kriging (OK) was used as an interpolation method. In this study, a minimum of 8 neighbours was used within a circular search area with a radius of 20 m around the location being interpolated. The spatial structure of the variables was represented by variogram models, which were used to assign weights to the neighbouring points.

2.4. Resistivity imaging

Geo-electrical imaging was done with the ABEM Terrameter and Lund electrode selector system (ABEM instrument AB, Sundbyberg, Sweden). With this multi-electrode resistivity system, 64 electrodes were arranged in a straight line with a constant spacing of 1 m and connected to a multi-core cable. A controller system selected the combination of four active electrodes for each measurement of the resistivity data. The combined Wenner-Schlumberger electrode configuration was chosen because it has a better horizontal coverage than the Wenner array. The Wenner–Schlumberger array shows a fair sensitivity to horizontal and vertical features (Kaufmann and Cerak, 2001).

The data obtained were first interpreted using RES2DINV software (Loke et al. (2003)) to determine a two-dimensional resistivity model for the subsurface which produces a pseudosection that agrees with the actual measurements (Geotomo software, 2007). The distance for the electrode configuration midpoint was plotted against the electrode separation for each measured data point, reflecting the measurement depth. The corresponding apparent resistivity along the vertical section allowed geological boundaries to be identified, by characterizing the ground in terms of the thickness of individual layers together with their respective apparent resistivity values along the vertical profile (Batte et al., 2008).

If the layering of the soil is known, the purpose of an 1D-inversion subroutine exists in determining the thickness and the resistivity of the different layers. We used RES1D (Loke, 2001) for this purpose. In this method, an initial model must be given, and the optimisation subroutine modifies the thickness and resistivity of the layers so as to reduce the difference between the calculated and measured apparent resistivity values.

2.5. EC-probe

The standard EC-probe set for soil conductivity measurements consists of an EC-probe and an earth resistivity meter (Eijkelkamp Agrisearch Equipment, Giesbeek, The Netherlands). Measurement of the soil resistivity using four electrodes is based on the Wenner-method, described by Rhoades and Van Schilfgaarde (1976). The EC-probe measures in situ the electrical resistivity of a limited (elliptic) soil volume of 80 cm^3 of soil around the probe. A temperature sensor is used to convert the measurements to a reference temperature. This sensor can be used only for a limited number of punctual measurements. Moreover, these act as calibration measurements for the proximal soil sensing data.

2.6. Depth response curves

In a two-layered soil model where silty loess is situated above a clayey substrate, the relationship between z_{clay} and the ECa can be modelled by formulating the cumulative response $R_p(z_{clay})$ for the perpendicular coil orientation and $R_v(z_{clay})$ for the vertical coil orientation. Doolittle et al. (1994), Cockx et al. (2007) and Vitharana et al. (2008) fitted exponential regression models to their z_{clay} & ECa observations. Depths are normalized by dividing the z_{clay} by the intercoil spacing s to remove the effect of differences in intercoil spacing into our cumulative response functions $R_p(z_{clay})$ and $R_v(z_{clay})$ (Morris, 2009):

$$R_p(z_{clay}) = \alpha_p \cdot e^{-\beta_p \cdot \left(\frac{z_{clay}}{s}\right)} \quad (1)$$

$$R_v(z_{clay}) = \alpha_v \cdot e^{-\beta_v \cdot \left(\frac{z_{clay}}{s}\right)} \quad (2)$$

with α_p and β_p the unknown parameters of the exponential cumulative response function for the perpendicular coil configuration $R_p(z_{clay})$ and α_v and β_v the unknown parameters of the exponential cumulative response function for the vertical coil configuration $R_v(z_{clay})$. These unknown parameters α_p and β_p will be empirically determined by fitting the cumulative response function $R_p(z_{clay})$ to the z_{clay} & $ECa_{p,1.1}$ and z_{clay} & $ECa_{p,2.1}$ observations and α_v and β_v will be determined by fitting the cumulative response function $R_v(z_{clay})$ to the z_{clay} & $ECa_{v,1}$ and z_{clay} & $ECa_{v,2}$ observations. The procedure used to fit $R_p(z_{clay})$ to the z_{clay} & $ECa_{p,1.1}$ measurements is described here.

The cumulative responses from the upper and lower layers are $1-R_{p,s}(z_{clay})$ and $R_{p,s}(z_{clay})$, with s the intercoil spacing. For every z_{clay}, the corresponding $ECa_{p,1.1}$ and $ECa_{p,2.1}$ can be expressed as a function of the apparent conductivity values of the Quaternary loess and Tertiary clay (EC_{loess} and EC_{clay} respectively), taking the height of the DUALEM-21S sensor above the soil surface (0.16 m) into account:

$$ECa_{p,1.1} = \left[R_{p,1.1}(0.16) - R_{p,1.1}\left(z_{clay}\right)\right] \cdot EC_{loess} + \left[R_{p,1.1}\left(z_{clay}\right)\right] \cdot EC_{clay} \quad (3)$$

$$ECa_{p,2.1} = \left[R_{p,2.1}(0.16) - R_{p,2.1}\left(z_{clay}\right)\right] \cdot EC_{loess} + \left[R_{p,2.1}\left(z_{clay}\right)\right] \cdot EC_{clay} \quad (4)$$

Based on Eqs. (3) and (4), z^*_{clay} can be modelled given the $ECa_{p,1.1}$ and $ECa_{p,2.1}$ measurements. Therefore, $R_{p,1.1}(z^*_{clay})$ and $R_{p,2.1}(z^*_{clay})$ were calculated given the ECa measurements and the conductivities of the two layers (EC_{loess} and EC_{clay}):

$$R_{p,1.1}\left(z^*_{clay}\right) = \frac{ECa_{p,1.1} - R_{p,1.1}(0.16) \cdot EC_{loess}}{EC_{clay} - EC_{loess}} \quad (5)$$

$$R_{p,2.1}\left(z^*_{clay}\right) = \frac{ECa_{p,2.1} - R_{p,2.1}(0.16) \cdot EC_{loess}}{EC_{clay} - EC_{loess}} \quad (6)$$

These calculated $R_{p,1.1}(z^*_{clay})$ and $R_{p,2.1}(z^*_{clay})$ can be put into Eqs. (1) and (2) to obtain the modelled z^*_{clay}:

$$z^*_{clay} = -\frac{s}{\beta_p} \cdot ln\left(\frac{R_{p,1.1}\left(z^*_{clay}\right)}{\alpha_p}\right) - 0.16 \quad (7)$$

$$z^*_{clay} = -\frac{s}{\beta_p} \cdot ln\left(\frac{R_{p,2.1}\left(z^*_{clay}\right)}{\alpha_p}\right) - 0.16 \quad (8)$$

To fit a cumulative depth response function to the to the z_{clay} & $ECa_{p,1.1}$ and z_{clay} & $ECa_{p,2.1}$ data points, the sum of the squared differences between z_{clay} and z^*_{clay} was minimized, simultaneously for both the 1.1P and 2.1P coil configurations:

$$\sum_{i=1}^{n}\left[z_{clay}(i) - z^*_{clay}(i)\right]^2 = min \quad (9)$$

with i the number of the observation and n the total amount of observations. The parameters of the cumulative response function α_p and β_p were iteratively adjusted to obtain the smallest sum of the squared differences between z_{clay} and z^*_{clay} for both the 1.1P and 2.1P coil configurations.

The same approach was followed to fit a cumulative depth response function to the z_{clay} & $ECa_{v,1}$ and z_{clay} & $ECa_{v,2}$ observations, resulting in unique parameters α_v and β_v for the response function of the vertical coil configuration.

This minimization procedure was performed for both perpendicular coil configurations together and for both vertical coil configurations together. The difference between observed and modeled z_{clay} was simultaneously minimized for both 1.1P and 2.1P coil configurations and simultaneously for both 1 V and 2 V coil configurations.

2.7. Depth modelling

In a two-layered soil build-up, the measured ECa can be estimated by summing the conductivities and contributions of each layer. The following four equations can be formulated (Saey et al., 2009a,b):

$$ECa_{p,1.1} = \left[R_{p,1.1}(0.16) - R_{p,1.1}\left(z^*_{clay} + 0.16\right)\right]\cdot EC_{loess} + \left[R_{p,1.1}\left(z^*_{clay} + 0.16\right)\right]\cdot EC_{clay} \quad (10)$$

$$ECa_{p,2.1} = \left[R_{p,2.1}(0.16) - R_{p,2.1}\left(z^*_{clay} + 0.16\right)\right]\cdot EC_{loess} + \left[R_{p,2.1}\left(z^*_{clay} + 0.16\right)\right]\cdot EC_{clay} \quad (11)$$

$$ECa_{v,1} = \left[R_{v,1}(0.16) - R_{v,1}\left(z^*_{clay} + 0.16\right)\right]\cdot EC_{loess} + \left[R_{v,1}\left(z^*_{clay} + 0.16\right)\right]\cdot EC_{clay} \quad (12)$$

$$ECa_{v,2} = \left[R_{v,2}(0.16) - R_{v,2}\left(z^*_{clay} + 0.16\right)\right]\cdot EC_{loess} + \left[R_{v,2}\left(z^*_{clay} + 0.16\right)\right]\cdot EC_{clay} \quad (13)$$

with $R_{p,s}(z)$ and $R_{v,s}(z)$ the responses above a depth z for the perpendicular and vertical dipole mode respectively.

3. Results and discussion

3.1. ECa survey with the DUALEM-21S sensor

Table 1 shows the summary statistics of the four ECa measurements taken with the DUALEM-21S sensor at 209 400 locations. The mean and maximum values of the ECa values increase with increasing DOE (Saey et al., 2009a), so the larger the measured soil volume, the higher the conductivity. The negative minimum values of $ECa_{p,1.1}$ and $ECa_{p,2.1}$ were assumed to be caused by small metal objects in the subsoil. The standard deviations increase with increasing DOE, because of the higher differences in absolute values. Fig. 2 shows the $ECa_{v,1}$ measurements of the study area converted to a reference measurement temperature of 25 °C. The parameters of the $ECa_{v,1}$ variogram model are given in Table 2. Large differences of $ECa_{v,1}$ were observed across the study area, probably due to depth variations of the higher conductive subsoil.

Table 1
Descriptive statistics (m: mean, min: minimum, max: maximum, std: standard deviation) of $ECa_{p,1.1}$, $ECa_{p,2.1}$, $ECa_{v,1}$ and $ECa_{v,2}$ for the 209 400 measurements in the study area (in mS m^{-1} after conversion to a reference temperature of 25 °C).

Variable	m	Min	Max	Std
$ECa_{p,1.1}$	33	−22	108	13
$ECa_{p,2.1}$	56	−35	164	22
$ECa_{v,1}$	65	2	176	26
$ECa_{v,2}$	85	33	230	30

3.2. Observations of the depth-to-clay

The locations of the z_{clay} observations within the test area were shown on Fig. 2. This test area was taken because of the high differences in ECa values on a relatively short distance and was supposed to be representative for the entire study area. Two transects DEFG and HI and one 30 m by 30 m grid (Fig. 2) were laid out within our test area in such a way that higher and lower ECa measurements of the test field were visited (Fig. 2) (Saey et al., 2008). Along the 225 m of transect DEFG 46 observation points were located at 5 m intervals, while along transect HI 15 points were selected at 3 m intervals. 24 observation points were located on a 30 m by 30 m grid.

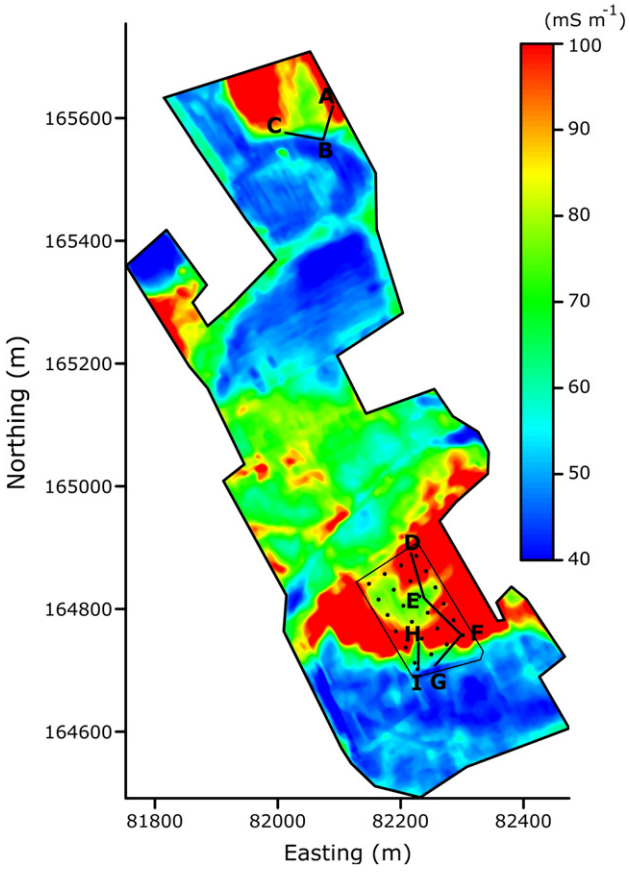

Fig. 2. Kriged apparent electrical conductivity map (converted to a reference temperature of 25 °C) in the 1 m — vertical coil configuration ($ECa_{v,1}$) with localization of transects AB, BC, DEFG and HI and the 30 m by 30 m grid. The border of the test area is denoted with a black frame.

Table 2
Parameters of the variogram model for $ECa_{v,1}$, X and z^*_{clay} (C_0: nugget variance; C_1: sill and a: range).

Variable	Type	C_0	C_0+C_1	Slope	a (m)
$ECa_{v,1}$ (mS m^{-1})	Linear	0	–	4.2	–
X (m)	Gaussian	0.0005	1.7005	–	30
z^*_{clay} (m)	Gaussian	0.004	1.559	–	30

At each of these 85 points, z_{clay} was observed by augering with a gouge auger. At the last four sampling points of transect DEFG and the last sampling point of transect HI, the loess layer extended beyond a depth of 3.5 m, which was our maximal augering depth. These observations were not taken into account for the calculation of the depth response curves.

With these 80 depth observations, the cumulative response curves for the perpendicular and vertical coil configurations were fitted. Table 3 shows that on the 225 m transect DEFG, z_{clay} is on average relatively shallow (0.79 m), with a variation between 0.12 m to 1.57 m, similarly to the spread of the z_{clay} observations on the 30 m by 30 m grid (0.15 m to 1.81 m). On the 45 m transect HI, z_{clay} increases from 1.52 m to 2.82 m.

3.3. Punctual EC-measurements

With the EC-probe, EC measurements of the two layers were conducted according to a 30 m by 30 m grid on the test area (Fig. 2). The average EC of the loess layer (EC_{loess}) was 21 ± 6 mS m^{-1} (12 measurements) and of the clayey layer (EC_{clay}) it was 192 ± 13 mS m^{-1} (7 measurements), at 25 °C. These values were taken to be representative for the two different layers across the study area.

3.4. Fitted depth response functions

The fitting of the depth response functions was done by minimizing the sum of the squared differences between z_{clay} and z^*_{clay} by iteratively altering the modelling parameters α_p and β_p for both perpendicular coil configurations and by altering parameters α_v and β_v for both vertical coil configurations.

The optimal values of α_p and β_p were 0.8135 and 1.4131 and 0.9802 and 0.8102 for α_v and β_v. The obtained empirical depth response curves were:

$$R_{p,s}(z_{clay}) = 0.8135\cdot e^{-1.4131\cdot\left(\frac{z_{clay}}{s}\right)} \quad (14)$$

$$R_{v,s}(z_{clay}) = 0.9802\cdot e^{-0.8102\cdot\left(\frac{z_{clay}}{s}\right)} \quad (15)$$

with $R_{p,s}(z)$ and $R_{v,s}(z)$ the responses above a depth z for the perpendicular and vertical dipole mode and transmitter-receiver coil spacing s. The DOE for the fitted cumulative depth response functions were 0.62 m and 1.32 m for the 1.1P and 2.1P coil configurations and 1.30 and 2.76 m for the 1 V and 2 V coil configurations. Fig. 3 shows the cumulative response curves (expressed as z_{clay} & ECa relationship (Eqs. (2) and (3)) given the conductivities of the different layers EC_{loess} and EC_{clay}) plotted against their 80 corresponding z_{clay} & ECa observations. The modelled response curves coincide well with the z_{clay} & ECa observations. Coefficients of determination (R^2) are 0.74 and 0.77 for the 1.1P and 2.1P coil configurations and 0.65 and 0.68 for the 1 V and 2 V coil configurations. Only the low $ECa_{v,1}$ observations underestimate the real z_{clay}. Below an ECa of about 20 mS m^{-1} for the 1.1P coil configuration, z_{clay} changes largely with small changes in ECa. Therefore, this depth response curve is inappropriate to predict the deeper z_{clay}. The inverse situation can be observed with regard to the 2 V configuration. This configuration shows an almost linear z_{clay} & ECa trend below a value of about 90 mS m^{-1}, confirming the sensitivity of the 2 V coil configurations for deeper z_{clay}.

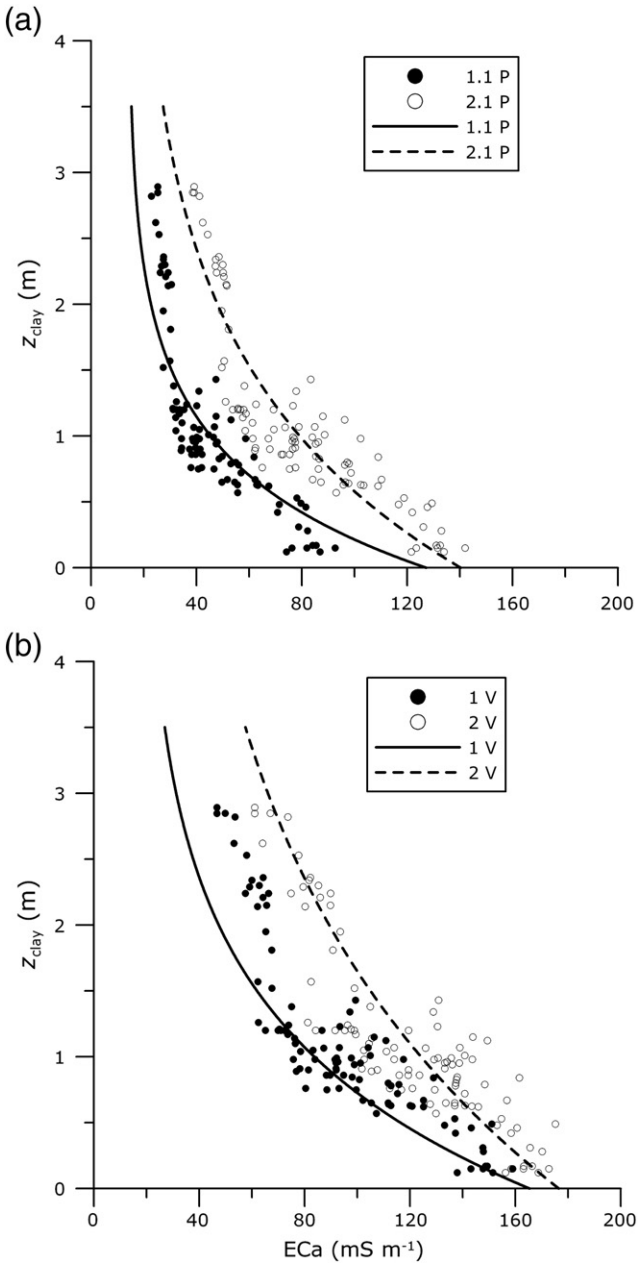

Fig. 3. Fitted cumulative depth response curves (and expressed as depth-to-clay (z_{clay}) — apparent electrical conductivity (ECa) relationship) (a) for the perpendicular coil configurations and (b) the vertical coil configurations of the DUALEM-21S, each with their corresponding z_{clay}-ECa observations.

Table 3
Descriptive statistics (n: number, m: mean, min: minimum, max: maximum, std: standard deviation) of z_{clay} at the test field.

	n	m (m)	Min (m)	Max (m)	Std (m)
Transect DEFG	42	0.79	0.12	1.57	0.39
Transect HI	14	2.26	1.52	2.82	0.30
Grid	24	0.89	0.15	1.81	0.36

3.5. Depth modelling

The four simultaneous ECa measurements obtained with the quadruple-array DUALEM-21S sensor were combined to model and map z_{clay}. The conductivities of the loess and clayey layer were taken from the EC-probe measurements and assumed homogeneous across the study area. Finally, the system of Eqs. (10)–(13) could be solved to model z^*_{clay} at each of the 209 400 measurement locations, by applying $R_{p,s}(z)$ and $R_{v,s}(z)$ from Eqs. (14) and (15) and $EC_{loess} = 21$ mS m^{-1} and $EC_{clay} = 192$ mS m^{-1}. This system was solved with Matlab using the Levenberg–Marquardt algorithm (Marquardt, 1963).

3.6. Validation

The accuracy of the proposed model to predict z^*_{clay} was evaluated by using the 1D-inverted depths at the 2 transects AB and BC located in a different part of the study area but with an analogeous range of ECa values as the test area (Fig. 2). 1D inversion was done given an initial model representing a two-layered soil with resistivity of the topsoil much higher than that of the subsoil. This initial model was confirmed by the 2D-transect modelling (Fig. 4). EC^*_{loess} and EC^*_{clay} were also modelled at each measurement location. They were found to be relatively stable, except near the borders of the transects, which was due to less resistivity measurements. The average EC^*_{loess} and EC^*_{clay} were 28 and 194 mS m^{-1}, which corresponded well to the values measured with the EC probe (21 and 192 mS m^{-1}). At these 95 locations, the 1D-inverted depths were compared with the modelled depths (Fig. 5).

The MEE and RMSEE were respectively 0.08 m and 0.22 m. In order to compare the RMSEE or the accuracy of prediction between variables of different type, the RMSEE can be normalized by the total variation, by dividing it to the standard deviation of the observations (in this case 0.67 m). As a rule of thumb, Hengl et al. (2003) considered that a value of relative RMSEE close to 40% means a fairly satisfactory accuracy of prediction. Otherwise, if the values get >71%, this means that the model accounted for less than 50% of variability at the validation points and the prediction is unsatisfactory. In this case, the relative RMSEE is 33%, certainly accurate enough for hydrological modelling. The R^2 between z_{clay} and z^*_{clay} was 0.95, which

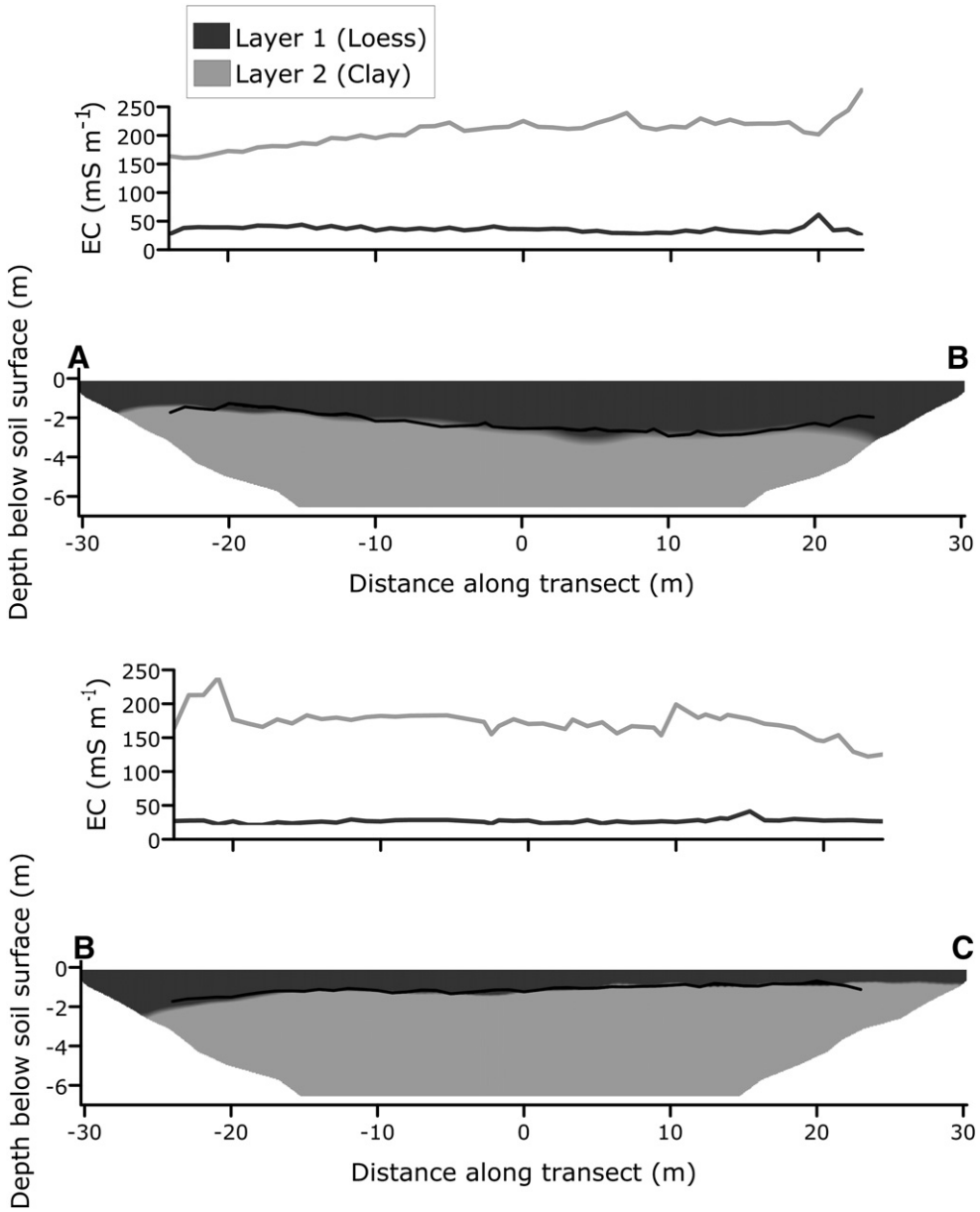

Fig. 4. 2D-inverted transects with 1D-inverted depths of the interface between the loess and clay (black line) and the corresponding modelled conductivities of the loess (EC_{loess}) and clay (EC_{clay}) for transects AB and BC.

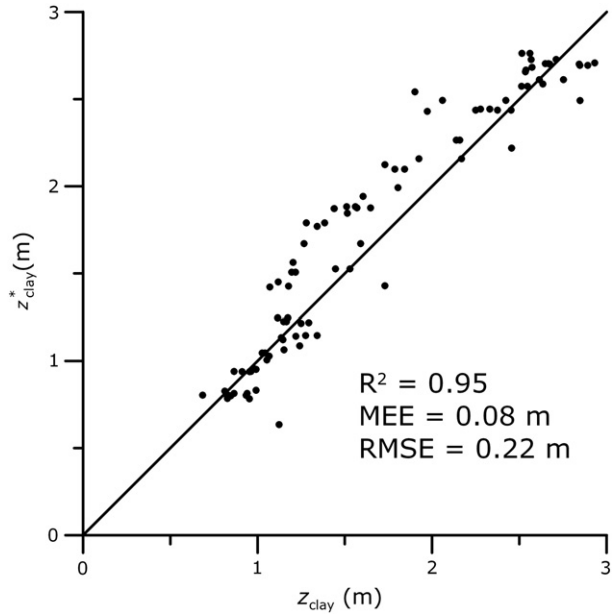

Fig. 5. Scatterplot of the predicted clay depth (z^*_{clay}) versus the observed depth (z_{clay}) with validation indices.

is highly significant at $\alpha = 0.05$. Therefore, the modelled relationship was found to have a negligible bias, to be reasonably accurate and to correlate well with the observed depths. Moreover, the formulated cumulative depth response curves prove to be useful for modelling the depth to the interface in a two-layered soil.

3.7. Paleolandscape beneath the loess cover

The soil surface elevation (X) of the fields was gathered with LIDAR and visualized in Fig. 6(a). At each location, the 4 ECa measurements were converted into z^*_{clay} using the set of (Eqs. (10)–(13)) given the fitted depth response curves (Eqs. (14) and (15)). The interpolated map of z^*_{clay} was subtracted from X and the resulting X-z^*_{clay} elevations are given in Fig. 6(b). To investigate the large variation in thickness of the loess cover, z^*_{clay} is displayed in Fig. 6(c). The kriging interpolations were carried out similarly to the $ECa_{v,1}$ but with a different variogram model (parameters given in Table 2). When comparing the current topography (Fig. 6(a)) with the paleolandscape beneath the loess cover (Fig. 6(b)), it will be clear that the paleolandscape is much more variable. Different gully systems occur on the paleorelief and are very pronounced on both sides of ridge B onto the Tertiary surface (Fig. 6(b)). When comparing the current elevation (Fig. 6(a)) with the paleolandscape (Fig. 6(b)), the boundary between the southern en northern watersheds differs. This was indicated on Fig. 6(a) and (b) with the dashed lines. The watershed boundary onto the paleolandscape cannot be correlated to the boundary on the current elevation due to the uneven loess cover near this boundary. Therefore, subsurface flow onto the paleolandscape will not coincide with the surface runoff. North of this watershed boundary, a small plateau (A) occurs onto the Tertiary surface (Fig. 6(b)) with a wide gully around it. To evaluate the continuity of these flow pathways, the Idrisi Kilimanjaro (Clark Labs, Worcester, MA, U.S.A.) modules RUNOFF (Jenson and Domingue, 1988) and WATERSHED were applied to the paleolandscape. With this analysis, current and subsurface or past flow patterns were obtained and visualized in both Fig. 6(a) and (b). Comparing the current and past flow lines confirms the above observations about the watershed boundaries. Ridge B shows to be more pronounced on the Tertiary surface, because a flowline was

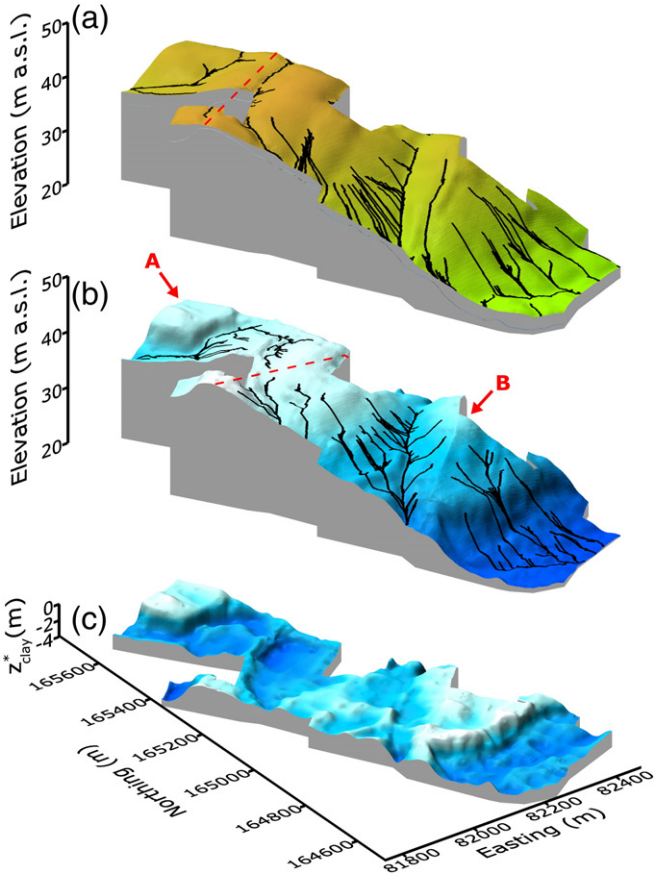

Fig. 6. (a) The elevation of the current surface with modelled flow patterns and (b) the elevation of the paleolandscape before the deposition of the loess cover with modelled flow patterns and (c) 3D-surface of the modelled depth-to-clay (z^*_{clay}).

modeled across it on the current surface (Fig. 6(a)). In general, the flowlines do not to coincide on places with large variations in z^*_{clay}. Water that percolates through the loess cover flows from both flanks of ridge B and will accumulate in a gully at both sides of it. The wide gully around plateau A could also serve as a surface drainage path for the higher part of the study area.

4. Conclusions

The presented methodology presents an application of the prediction of sensor depth response curves in a two-layered soil. The depth response curves of an EMI instrument with multiple coil configurations were calculated in a rapid, effective and accurate way (R^2 of 0.74 and 0.77 for the perpendicular coil configurations; R^2 of 0.65 and 0.68 for the vertical coil configurations). Finally, the depth-to-clay was modelled accurately (R^2 of 0.95 and RMSEE of 0.22 m), which allowed the detailed reconstruction of the paleolandscape beneath the loess cover. Flowlines visualized on this Tertiary surface represented past or subsurface drainage paths.

Acknowledgements

This research was supported by the Fund for Scientific Research-Flanders (FWO-Vlaanderen). The authors thank Hans Vermeersch and Valentijn Van Parys for executing the field work and thank Mr. Eddy Hooghe, Mr. Michel Coussement, Mr. Rik Vandeputte and Mr. Luc Vandesteene for granting access to their fields.

References

Batte, A., Muwanga, A., Owor, M., 2008. Vertical electrical sounding as an exploration technique to improve on the certainty of groundwater yield in the fractured crystalline basement aquifers of eastern Uganda. Hydrogeology Journal 16, 1683–1693.

Callegary, J.B., Ferré, Ty P.A., Groom, R.W., 2007. Vertical spatial sensitivity and exploration depth of low-induction-number electromagnetic-induction instruments. Vadose Zone Journal 6, 158–167.

Cockx, L., Van Meirvenne, M., De Vos, B., 2007. Using the EM38DD soil sensor to delineate clay lenses in a sandy forest soil. Soil Science Society of America Journal 71, 1314–1322.

Domsch, H., Giebel, A., 2004. Estimation of soil textural features from soil electrical conductivity recorded using the EM38. Precision Agriculture 5, 389–409.

Doolittle, J.A., Sudduth, K.A., Kitchen, N.R., Indorante, S.J., 1994. Estimating depth to clays using electromagnetic induction methods. Journal of Soil and Water Conservation 49, 572–575.

Dualem Inc., 2007. DUALEM-21S user's manual. Dualem Inc., Milton, Canada.

Geotomo Software, 2007. RES2DINV ver. 3.56. Rapid 2-D Resistivity & IP inversion using the least-squares method. .

Hendrickx, J.M.H., Borchers, B., Corwin, D.L., Lesch, S.M., Hilgendorf, A.C., Schlue, J., 2002. Inversion of soil conductivity profiles from electromagnetic induction measurements. Soil Science Society of America Journal 66, 673–685.

Hengl, T., Heuvelink, G.B.M., Stein, A., 2003. A generic framework for spatial prediction of soil variables based on regression-kriging. Geoderma 120, 75–93.

Hubert, P., 1976. Verklarende tekst bij het kaartblad: Zwevegem 97E. Hoste-Staelens, Gent.

Hufty, A., 2001. Introduction à la climatologie. De Boeck Université, Brussels.

Jenson, S., Domingue, J., 1988. Extracting topographic structure from digital elevation data for geographic information system analysis. Photogrammetric Engineering and Remote Sensing 54, 1593–1600.

Kaufmann, O., Cerak, Y.Q., 2001. An application of cone penetration tests and combined array 2D electrical resistivity tomography to delineate cover-collapse sinkhole prone areas. In: Beck, B.F., Herring, J.G. (Eds.), Geotechnical and environmental applications of karst geology and hydrology. Swets & Zeitlinger Publishers, Lisse, The Netherlands, pp. 359–364.

Loke, M.H., 2001. RES1D ver. 1.0. 1-D Resistivity, IP & SIP Inversion and forward modelling.

Loke, M.H., Acworth, I., Dahlin, T., 2003. A comparison of smooth and blocky inversion methods in 2D electrical imaging surveys. Exploration Geophysics 34, 182–187.

Marquardt, D., 1963. An algorithm for least-squares estimation of nonlinear parameters. SIAM Journal of Applied Mathematics 11, 431–441.

McNeill, J.D., 1980. Electromagnetic terrain conductivity measurement at low induction numbers. Technical Note TN-6. Geonics Limited, Missisauga, Ontario, Canada.

Monteiro Santos, F.A., Triantafilis, J., Bruzgulis, K.E., Roe, J.A.E., 2010. Inversion of DUALEM-421 profiling data using a 1-D laterally constrained algorithm. Vadose Zone Journal 9, 117–125.

Morris, E.R., 2009. Height-above-ground effects on penetration depth and response of electromagnetic induction soil conductivity meters. Computers and Electronics in Agriculture 68, 150–156.

Pellerin, L., Wannamaker, P.E., 2005. Multi-dimensional electromagnetic modelling and inversion with application to near-surface earth investigations. Computers and Electronics in Agriculture 46, 71–102.

Reynolds, J.M., 1997. An Introduction to Applied and Environmental Geophysics. John Wiley & Sons Ltd., Chichester, England.

Rhoades, J.D., Van Schilfgaarde, J., 1976. An electrical conductivity probe for determining soil salinity. Soil Science Society of America Journal 40, 647–651.

Saey, T., Simpson, D., Vitharana, U., Vermeersch, H., Vermang, J., Van Meirvenne, M., 2008. Reconstructing the paleotopography beneath the loess cover with the aid of an electromagnetic induction sensor. Catena 74, 58–64.

Saey, T., Simpson, D., Vermeersch, H., Cockx, L., Van Meirvenne, M., 2009a. Comparing the EM38DD and DUALEM-21S Sensors for Depth-to-Clay Mapping. Soil Science Society of America Journal 73, 7–12.

Saey, T., Van Meirvenne, M., Vermeersch, H., Ameloot, N., Cockx, L., 2009b. A pedotransfer function to evaluate the soil profile textural heterogeneity using proximally sensed apparent electrical conductivity. Geoderma 150, 389–395.

Spies, B.R., Frischknecht, F.C., 1991. Electromagnetic Sounding. In: Nabighian, M.N. (Ed.), Electromagnetic methods in applied geophysics (volume 2, application, parts A and B). Society of Exploration Geophysicists, USA, pp. 285–426.

Tromp-van Meerveld, H.J., McDonnell, J.J., 2009. Assessment of multi-frequency electromagnetic induction for determining soil moisture patterns at the hillslope scale. Journal of Hydrology 368, 56–67.

Vitharana, U.W.A., Saey, T., Cockx, L., Simpson, D., Vermeersch, H., Van Meirvenne, M., 2008. Upgrading a 1/20, 000 soil map with an apparent electrical conductivity survey. Geoderma 148, 107–112.

Wait, J.R., 1962. A note on the electromagnetic response of a stratified earth. Geophysics 27, 382–385.

World Reference Base, 1998. World reference base for soil resources. World Resources Report, vol. 84. FAO, Rome, Italy.